Int. J. Electrochem. Sci., 14 **(2019)** 1909 – 1925, doi: 10.20964/2019.02.31

International Journal of ELECTROCHEMICAL SCIENCE
www.electrochemsci.org

Solid Polymer Electrolytes Based on Chitosan:NH_4Tf Modified by Various Amounts of TiO_2 Filler and its Electrical and Dielectric Characteristics

Shujahadeen B. Aziz [1,2,*], *Omed Gh. Abdullah* [1,2], *Shakahawan Al-zangana*[3]

[1] Prof. Hameed's Advanced Polymeric Materials Research Lab., Department of Physics, College of Science, University of Sulaimani, Qlyasan Street, Sulaimani, Kurdistan Regional Government-Iraq
[2] Komar Research Center (KRC), Komar University of Science and Technology, Sulaimani, 46001, Kurdistan Regional Government, Iraq
[3] Department of Physics, College of Education, University of Garmian, Kalar, Kurdistan Regional Government-Iraq
[*]E-mail: shujaadeen78@yahoo.com, shujahadeenaziz@gmail.com

Received: 29 August 2018/ *Accepted:* 10 October 2018 / *Published:* 5 January 2019

In the current work the role of titanium dioxide (TiO_2) filler on dielectric and conductivity properties of chitosan (CS) based solid polymer electrolytes (SPEs) were investigated at various temperatures. To prepare CS based SPEs fixed amount of ammonium triflate ($NH_4CF_3SO_3$) was dissolved in CS solution and then various amount of TiO_2 was added to CS: $NH_4CF_3SO_3$ solution. The films of composite electrolytes were obtained by solution cast technique. The results showed that dielectric properties of composite electrolytes have been improved up to 1 wt.% of TiO_2 and their values are found to be temperature dependent. The composite film incorporated with 1 wt.% of TiO_2 exhibits a smallest bulk resistance. The *M''* parameter against frequency shows asymmetric single relaxation peak which reveal the non-Debye relaxation type. The ac conductivity spectra were used to obtain the DC conductivity values at ambient temperature. The temperature dependent DC conductivity was found to follow Arrhenius behaviour. The obtained value of activation energies from DC conductivity is found to be comparable to that calculated from relaxation time. The single value of activation energy obtained from the Arrhenius plot indicates one conduction mechanism involved in the present system.

Keywords:proton ion conducting; solid polymer electrolytes; electric modulus; activation energy; relaxation process

1. INTRODUCTION

Nanocomposite electrolyte membranes are industrially important materials having extensive commercial applications in optoelectronic devices, chemical sensors, energy storage and memory elements[1-3]. Chitosan (CS) is an accessible natural polymer with a dopant dependent electrical and optical properties, due to its tremendous film-forming capability and good mechanical properties [4-6].

The amino (-NH_2) and hydroxyl (-OH) groups present in the CS backbone structure is enough to dissolve inorganic salts and formation of polymer electrolytes [7]. It is found that the structure, electrical and optical properties of fuctional polymers are changed by addition of metals and semiconductors particles such as cupper (Cu), sliver (Ag), aluminium (Al), zinc oxide (ZnO), tin dioxide (SnO_2), cadmium oxide (CdO), silver sulphide (Ag_2S), alumina (Al2O3) and titanium dioxide (TiO_2) [8-14]. Thus polymer composites are regarded as a potential candidate in electronic, optoelectronic and energy-storage devices [15,16]. The TiO_2 filler was one of the most widely investigated oxides. This is due to its wide range ofapplications including transparent conducting oxides (TCO) in LED's, resistive random access memory (RRAM), displays, and photovoltaic cells [17-19]. The TiO_2 is a direct bandgap semiconductor having an energy gap of 3.06 eV at room temperature. It was reported that the addition of TiO_2 filler to polymer electrolyte improves both the carrier transport propert and the mechanical strength of the component [20]. Several reports can be seen in literature on chitosan-based proton-conducting polymer electrolytes [21, 22]. The aim of this study is to reveal the role of TiO_2 filler on electrical properties of chitosan-ammonium triflate (CS-NH_4Tf) polymer electrolyte films. Dielectric properties and relaxation dynamics also was studied in detail.

2. EXPERIMENTAL DETAILS

Composite polymer electrolyte films of CS:NH_4Tf were prepared by solution cast technique. Low molecular weight chitosan (CS) supplied by Sigma-Aldrich was used as a host polymer without further purification. Ammonium triflate (NH_4Tf) salt was used as a source of proton ions. Acetic acid (1 vol.%) was used as the solvent in this work. For fabrication of polymer composites 1 g of CS powder was dissolved in 90 mL of acetic acid solution. To this solution, 30 wt.% NH_4Tf was added, and the mixture was stirred continuously to obtain a viscous solution. After that the necessary amount of dispersed inorganic TiO_2 filler was added to CS:NH_4Tf solution in wt.%. The solution was then transferred into the different dry Petri dishes and allowed the solvent to evaporate slowly at room temperature under vacuum for two weeks. The composite polymer electrolyte films were then relocated into desiccators for further drying before the test. The composite films were coded as CPT0, CPT1, CPT2, and CPT3, for CS-$NH_4CF_3SO_3$ incorporated with 0, 1, 3, and 5 wt.% TiO_2, respectively. The electrical conductivity and dielectric behaviour of composite polymer films were measured in the frequency range of 50 Hz – 1 MHz over a temperature ranges from 303K – 343K using a computer controlled HIOKI 3531 with a cell having two stainless steel blocking electrodes (2 cm in diameter) under spring pressure.

3. RESULTS AND DISCUSSION

3.1 Dielectric properties at ambient temperature

Previous investigations recognized that study of dielectric properties is crucial to understand the carrier transport properties and conductivity behaviour of polymer electrolytes [23-27]. The dielectric parameters are frequency dependent and they can be estimated using the following equations:

$$\varepsilon^* = \varepsilon' - j\varepsilon'' = \frac{Z_r}{\omega C_o(Z_r{}^2+Z_i{}^2)} - j\frac{Z_i}{\omega C_o(Z_r{}^2+Z_i{}^2)} \qquad (1)$$

Here, ε^* is complex permittivity with real $\varepsilon'$and imaginary ε''parts corresponding respectively to the storage and loss of energy in each cycle of the applied ac electric field. $Z_r$and Z_i are the real and imaginary part of impedance.$C_o = \varepsilon_o A/d$ is the vacuum capacitance, where ϵ_o is the vacuum permittivity, A is the sample cross-section area, and d is its thickness. The angular frequency ω is equal to $2\pi f$, where f is the frequency of applied field.

The frequency dependent of ε' andε'' parameters for various concentrations of TiO_2 filler are shown in Figures 1 and 2, respectively at ambient temperature. The dielectric response of all the samples under investigation, show one dispersion region and be inclined to diminish with increasing frequency. The results of dielectric properties point out that the polymer electrolyte incorporated with 1 wt.% TiO_2, has higher dielectric constant. The high value of ε' for CPT1 sample indicates the huge number of charge carriers, and thus it must exhibit a high conductivity. The study of impedance plots and ac conductivity may gives more information about the conductivity behaviour of the samples as can be seen in later sections.

The well-built dispersions of ε' and ε''at low down frequencies may be associated to the space-charge polarizations as a result of growth of immobile charge carriers at the electrode-electrolyte boundary [28]. However, at high frequencies, the space-charge growth disappeared. This can be understood based on the reality that the dipole moments and chare carriers cannot follow the high periodic reversal of the applied external ac electric field and thus there is no ion diffusion to the electrode-electrolyte interface [29, 30]. Consequently, a continuous decrease of the dielectric constants (ε' and ε'') expected with increase the frequency to high values. The temperature dependent dielectric properties may gives more information about the dispersion and plateau regions.

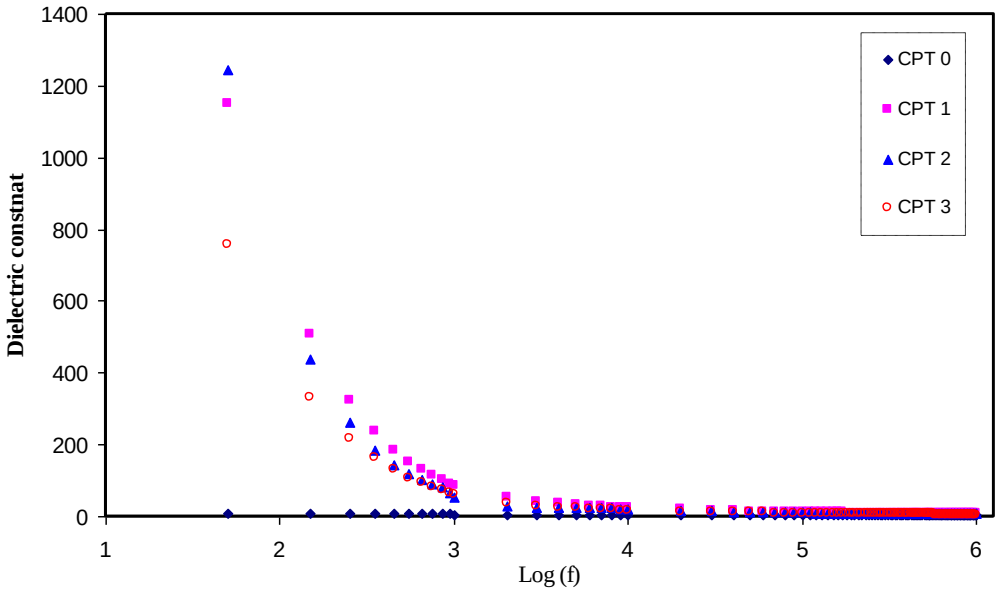

Figure 1. Concentration dependence of dielectric constant (ε') versus frequency at ambient temperature, for all composites.

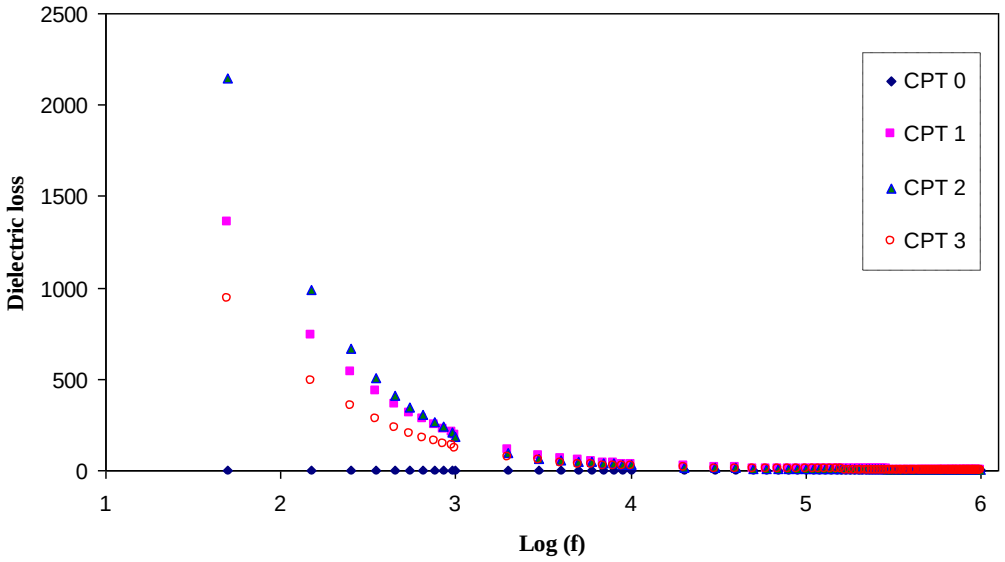

Figure 2. Concentration dependence of dielectric loss (ε'') versus frequency at ambient temperature, for all composites.

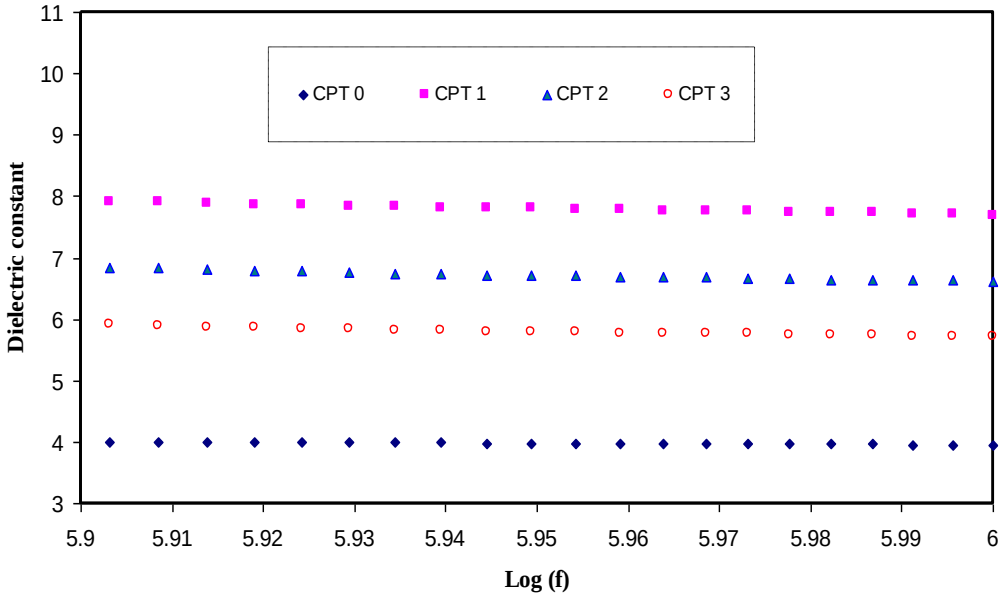

Figure 3. High-frequency dielectric constant as a function of frequency for all composites.

The variation of high-frequency region of bulk ε' as a function of frequency were illustrated in Figure 3. It can be seen noticeably that the high-frequency ε′ attains the maximum value for the hybrid film (CPT1) contained 1 wt.% of TiO_2. The high value of the static permittivity of composite films, can be discussed as follows; the TiO_2 filler possesses inherent strong ionic polarization due to quadruply charged Ti^{4+}cationand O^{2-} anions and therefore has a high value of static permittivity [31] and consequently more ions can be separated and their polarization gives a high dielectric constnat. Thus CPT1 sample shows an increase in permittivity due to an increase in both numbers of charge carriers and surface area. Furthermore, the increase of TiO_2 filler from 3 to 5 wt.% rediced the permittivity as a

consequence of aggregation of the nanoparticles and thus a decrease in the interface area. The increase of ε' can be interpreted based on the space charge polarization phenomena while its decrease is related to the blocking effect at high TiO_2 content and thus the aggregated filler particles acts as barriers for ion transport mechanism [23, 24, 28, 32]

To identify the relaxation dynamics associated with ion movement, complex electrical modulus formalism has been adopted. The analysis of electric modulus spectra can be considered as a well-organized method to characterize the relaxation behaviour of ionic materials [21, 33]. The complex electric modulus (M^*) is the reciprocal of the permittivity in the complex form [34, 35], and can be found as follows,

$$M^* = M_r + jM_i = \frac{\varepsilon'}{\left(\varepsilon'^2+\varepsilon''^2\right)} + j\frac{\varepsilon''}{\left(\varepsilon'^2+\varepsilon''^2\right)} \qquad (2)$$

where M_r and M_i are the real and imaginary parts of complex modulus. Figures 4 and 5, shows the frequency dependence of M_r and M_i respectively for all the composite electrolyte films. The observed small values of M_r and M_i at lower frequencies indicates the exclusion of electrode polarization involvement in electric modulus study [36]. It is valuable to note that the values of M_i show asymmetric broad peak in the high frequency regions which endorsed to the non-Debye behaviour. These peaks are correlated with the existence of high frequency semicircle of impedance plots. Thus impedance studies at various temperatures are helpful to understand the ion transport mechanism and relaxation processes.

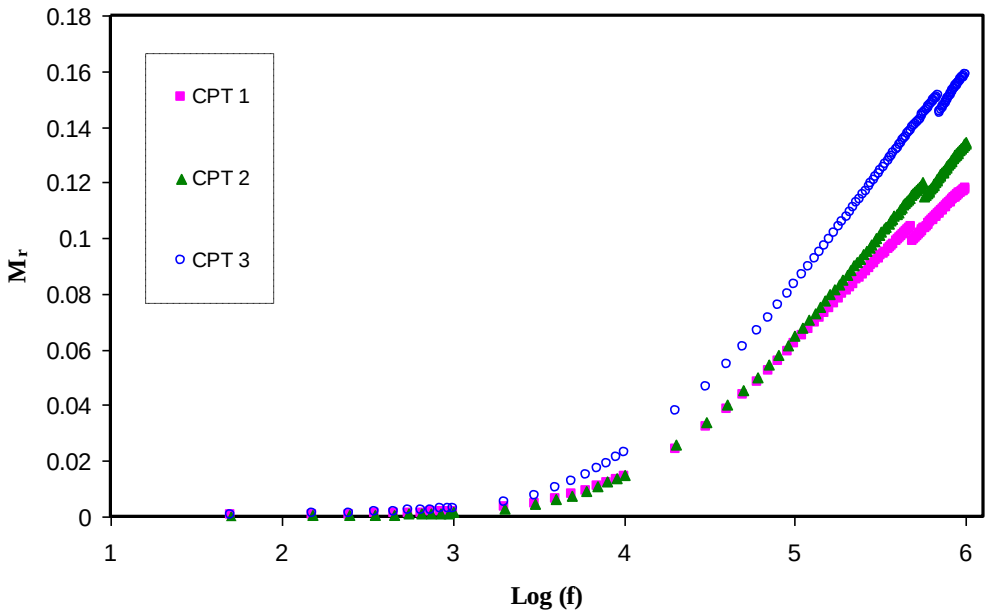

Figure 4. Variation of M_r as a function of frequency for polymer electrolyte composite samples, at ambient temperature.

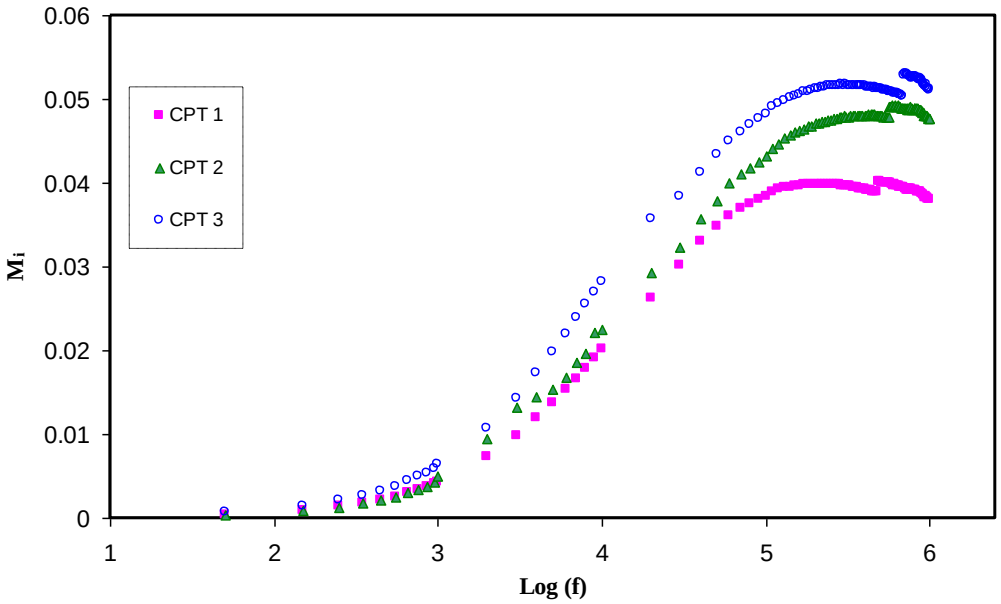

Figure 5. Variation of M_i as a function of frequency for polymer electrolyte composite samples at ambient temperature.

3.2. Impedance and AC conductivity study

Impedance study is an efficient approach for describing the electrical properties of the polymers and many composite materials [37]. Complex impedance plots offers a better understanding the nature of dielectric relaxation. The complex impedance spectroscopy analysis is significant to understand the conduction mechanism and the relaxation processes of the studied samples. Different relaxation processes take place in polymeric materials. When the relaxation times are owing to different mechanisms, the Nyquist plot will be asymmetrical arc [38].

Figure 6 represents the Cole-Cole plots of the studied composite films at room temperature. The Cole-Cole plots illustrate two noticeable regions: the high-frequency semi-circular arc and low-frequency tail. For a perfect Debye-type relaxation, a complete semicircle with its centre overlaps with the real axis (Zr) should be observed. But the results in Fig. 6 shows depressed semicircles whose centres are found below $Z_r$axis, which indicates the deviation from Debye-type behaviour [39, 40]. Distinctly, the CPT1 composite sample has minimum impedance, and hence it have a highest conductivity due to the contribution of huge amount of charge carriers to the conductivity. The increase of resistivity can be observed for the CPT2 and CPT3 samples. This can be attributed to the agglomeration of the TiO_2 filler which they act as barriers for ion transport, that is, a reduction of interface area and thus the ion carriers participating in conductivity decreased. This behaviour is in conformity with the results of dielectric analysis.

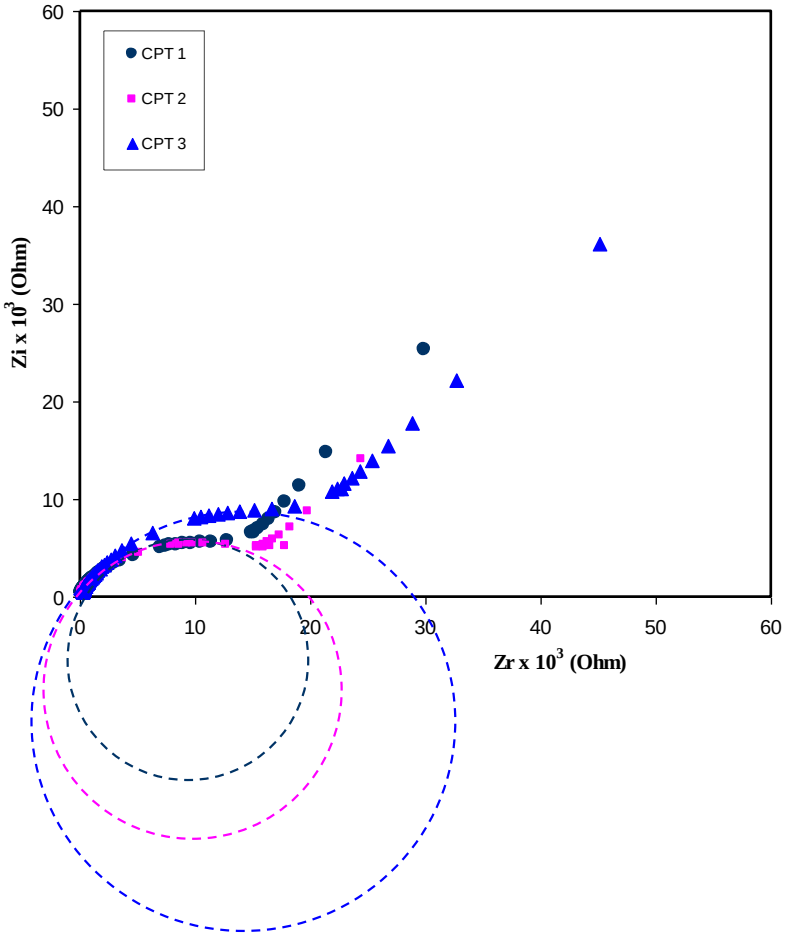

Figure 6. Cole-Cole plot of the studied composite films at room temperature.

The total conductivity $\sigma(\omega)$ has contribution from both the DC and ac part. The ac part is frequency-dependence and is given by Jonscher's power law [41, 42]

$$\sigma(\omega) = \sigma_{dc}(0) + \sigma_{ac}(\omega) = \sigma_{dc} + A\omega^{s} \qquad (3)$$

where $\sigma_{dc}(0)$ is the DC conductivity, A is the pre-exponential factor measures the strength of the polarizability, While, the plateau region of ac spectra can be considered for the estimation of the DC ($\sigma_{dc}(0)$) contribution. $\sigma_{ac}(\omega)$ is the dispersive ac conductivity, and s is the frequency exponent factor whose value lies between 0 and 1. Characteristic plots of σ_{ac} versus log (f) at room temperature for composite films are shown in Figures 7 (a-c). The σ_{ac} rises with raising the applied frequency for all studied samples which is similar to the behaviour of many organic-inorganic hybrid polymeric materials [43]. The high-frequency dispersion part related to ac conductivity (σ_{ac}), which is owing to trapped charges that are only dynamic at higher frequency region, whereas the intermediate frequency plateau section of the conductivity associated to the DC conductivity (σ_{dc}) which is frequency-independent due to the free ion motion within the composite sample [24, 28, 29]. The insets of Fig.7 show the obtained DC conductivity from the ac conductivity spectra which are in good agreement with the impedance plots

and dielectric constant results. Thus ac conductivity study can be regarded as a well-organized and specific plot to calculate approximately the DC conductivity.

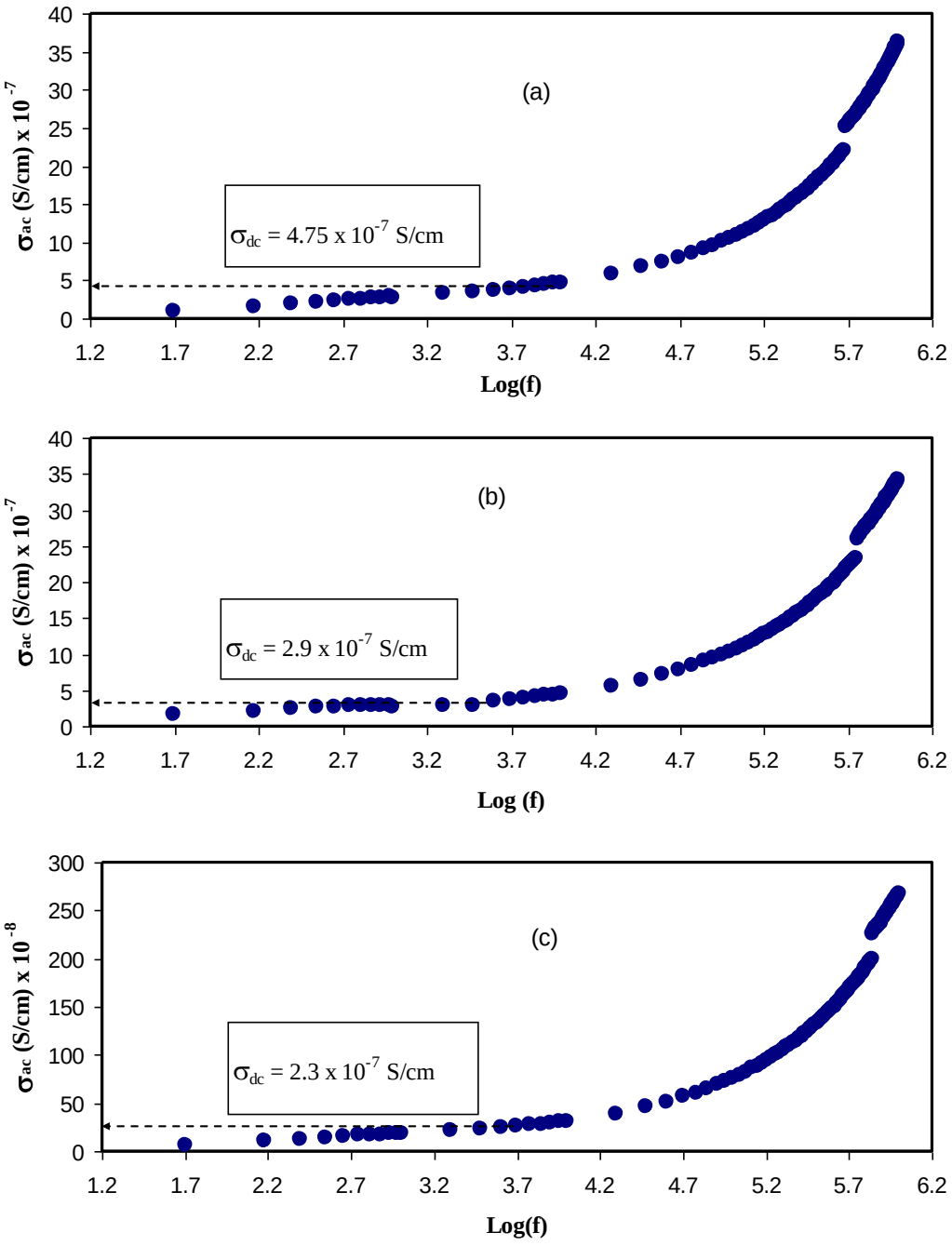

Figure 7. Variation of ac conductivity as a function of frequencyat room temperature for (a) CPT1, (b) CPT2, (c) CPT3 samples.

3.3 Dielectric properties as a function of temperature

Figure 8 demonstrate the ε' value as a function of frequency for CPT1 composite film at particular temperatures. The ε' is high at low frequencies and its value lowered with rising the applied frequency. The large value of ε' at low frequency region can be clarify based on Maxwell-Wagner model [44].The

TiO_2 doped polymer electrolyte samples consist of semiconducting islands in an insulating polymer matrix, and the dipoles are produced at the boundary of the two-components owing to the huge inequality in conductivities. These dipoles get polarized and therefore enhance the dielectric constant [45, 46]. At very high frequencies, the dipoles can no longer follow the applied field and $\varepsilon' \approx \varepsilon'_{\infty}$(high-frequency value of ε') [47]. Similar behaviour has been seen in several studies on polymer based nanocomposite films [48].

On the other hand, the dielectric constant increases monotonically with increasing temperature for all samples studied. For polar polymers such as CS, the increase of ε' with temperature is ascribed to the quick orientation of the dipoles and accordingly enhance the mobility of charge carriers [33, 38, 49].

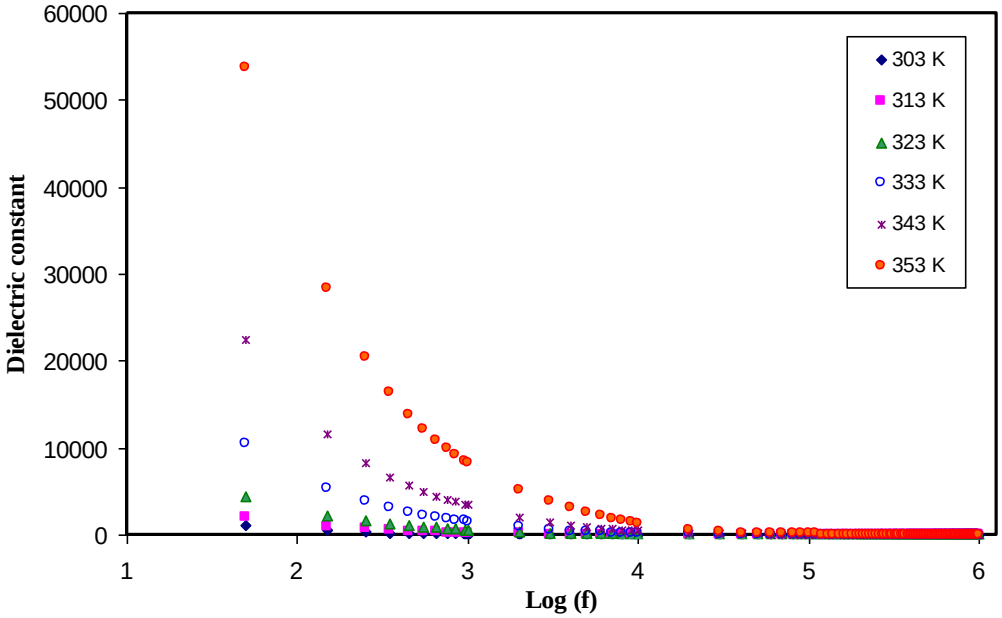

Figure 8. Frequency and temperature dependence of dielectric constant (ε') for CPT1 composite film at different temperatures

Figure 9 represent the variation of ε" as a function of frequency for CPT1 composite film at particular temperatures. Distinctly the ε" decline with increasing frequency and becomes small at high frequencies. At lower frequency region, due to Maxwell-Wagner-Sillars interfacial polarization effect, a big number of dipoles are trying to direct themselves along the field and therefore a big ε" value [50]. At higher frequency region, the periodic reversal of the electric field becomes so quick that permanent dipole molecules cannot direct themselves in reply to the external field. So, the charge accumulation lessens, leading to a decrease in ε" [6]. The increase of dispersion region in both ε' and ε" at high temperatures is attributed to the increase of charge carriers. It is well reported that at high temperatures the impedance plots almost show a slanted spike region which shows that the sample can be represented by a resistor [9, 24, 28]. To confirm this fact the impedance plots at various temperatures (323K to 353K) are shown in Figure 10. It is clear that the spike (tail) region due to electrode polarization (EP) increases at high temperatures. At high temperatures (Fig. 10b) the semicircles approximately disappeared. The diameter of semicircles at various temperatures was observed to be placed under the real axis, which point out that the related relaxation phenomena are of non-Debye type [51].

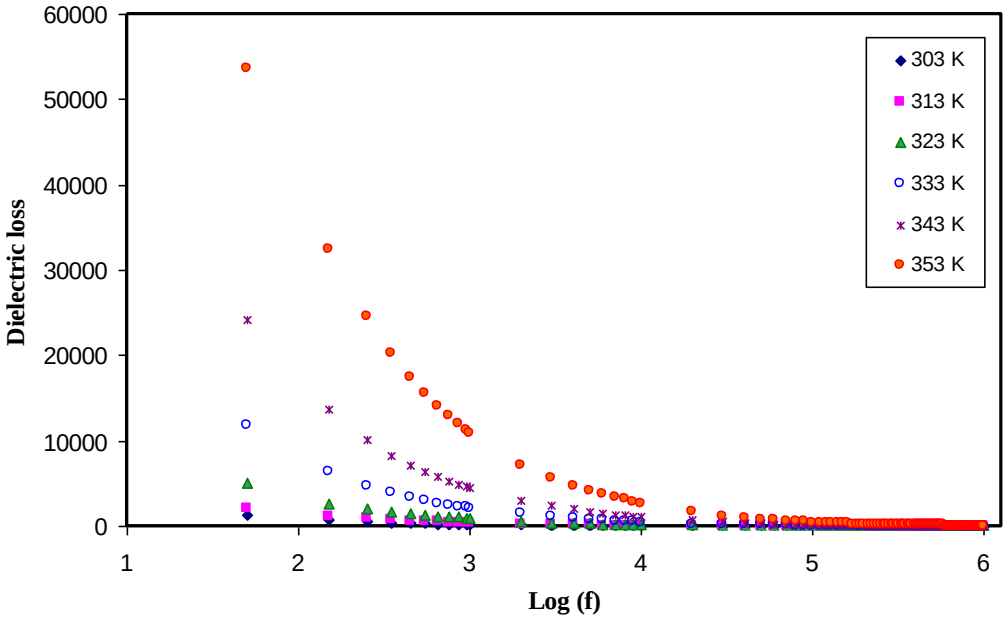

Figure 9. Frequency and temperature dependence of dielectric loss (ε") for CPT1 composite film at different temperatures.

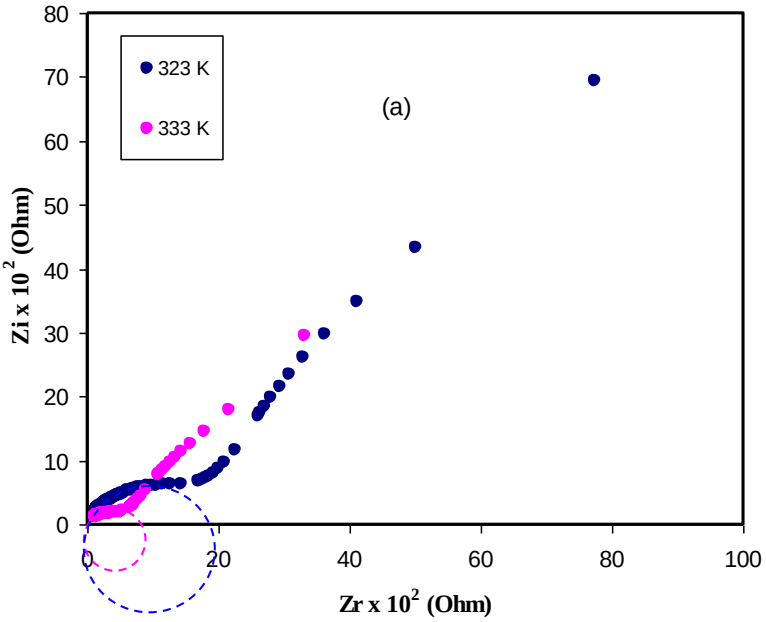

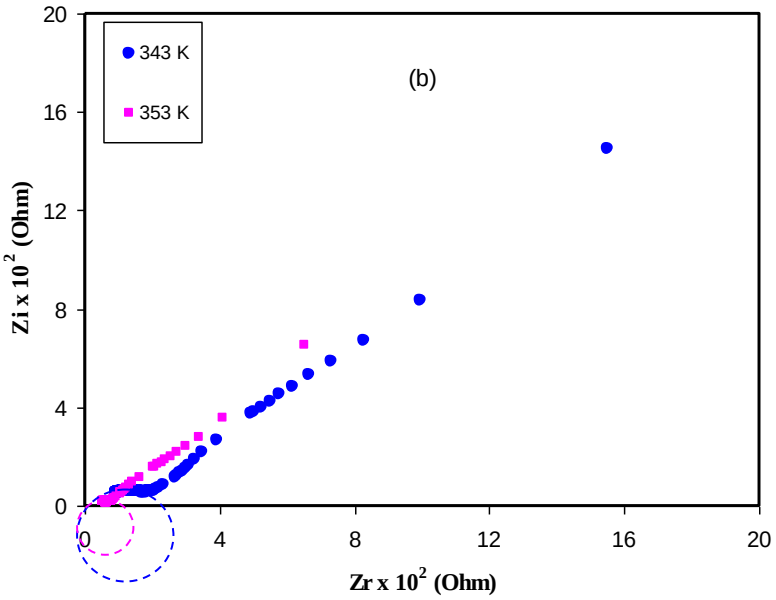

Figure 10. Impedance plots for CPT1 composite film at temperature ranges (a) 323-333 K, (b) 343-353 K.

Figure 11 represents the variation of M_r with frequency at particular temperatures for the CPT1 sample. It is observed that at low frequencies, the values of M_r are almost zero. This observation may possibly be related to a lack of restoring force governing the charge carrier mobility under the action of an induced electric field [38, 52]. Low M_r values at low frequencies at particular temperatures, point out to the nonexistence of noticeable electrode polarization [44, 52].

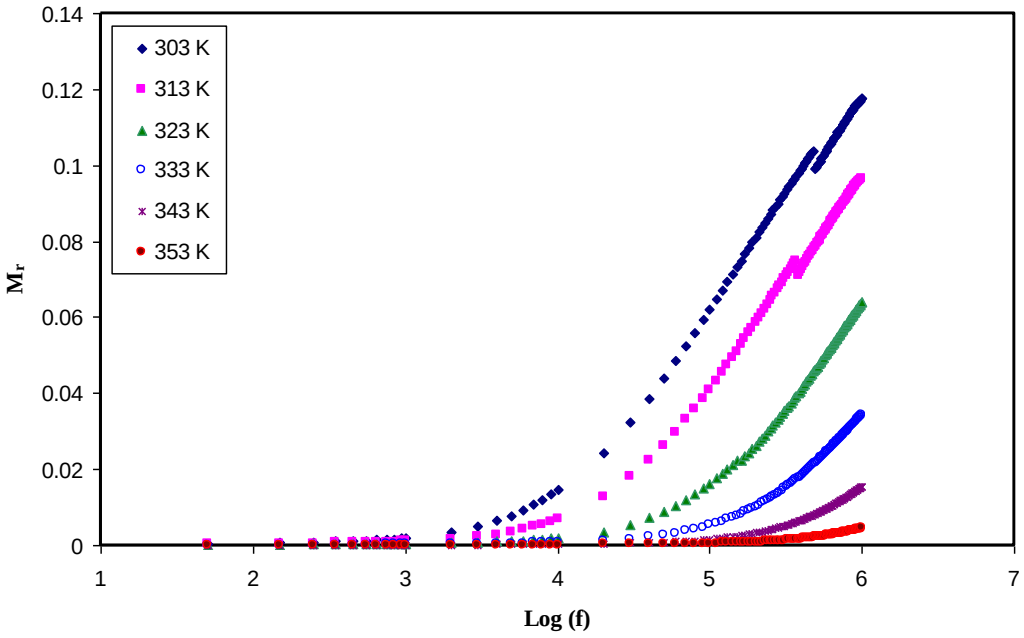

Figure 11. Real part of the electric modulus (M_r) as a function of frequency at selected temperatures for CPT1 composite film.

The spectrum of M_i at particular temperatures for the CPT1 sample is given in Fig. 12. The curves in Fig. 12 demonstrate that the $M_i$values arrive to a greatest value at a particular frequency and after that diminish with increasing frequency. It is obvious from the spectra that the maximum peak moves to the higher frequency side with temperature elevation. The regions beside the maximum peaks are not the same and this is reveals the departure from the ideal Debye-type behaviour. The shift of the ($M_{i_{max}}$) peaks towards the higher frequencies recommend a decrease in relaxation time, which directly enhances the ion mobility and hence the electrical conductivity [53].

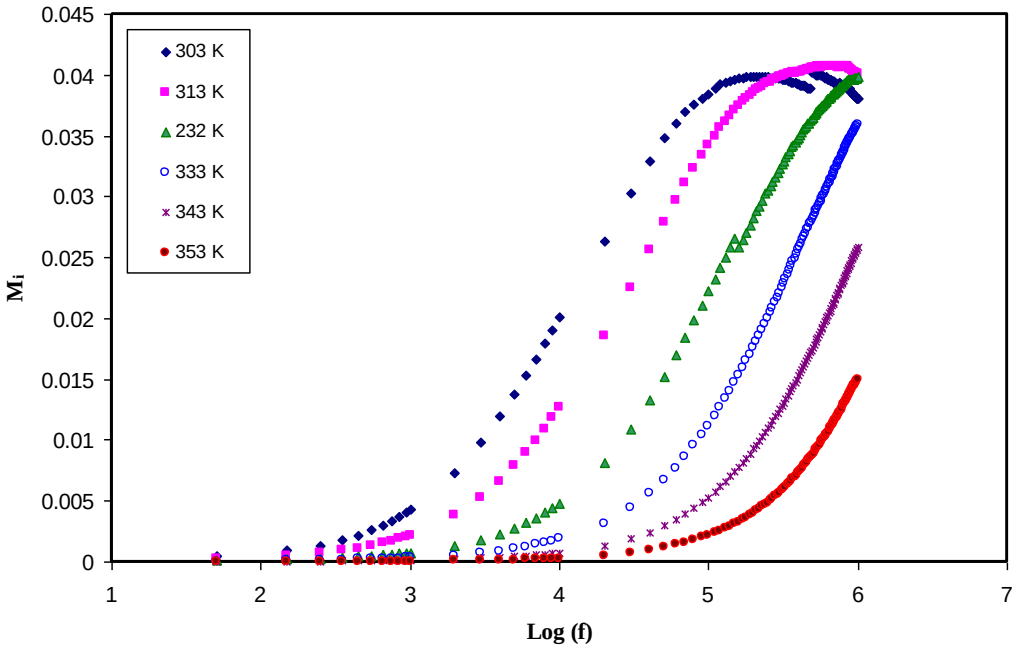

Figure 12. Imaginary part of the electric modulus (M_i) as a function of frequency at selected temperatures for CPT1 composite film.

3.4 Ion transport mechanism and activation energy

It was shown form impedance plots and ac spectra that CPT1 sample exhibits the highest DC conductivity. From the impedance plots at different temperatures the bulk resistance was determined. The thickness of the sample and it effective area were used to calculate the DC conductivity at various temperatures. The obtained values of DC conductivity versus temperature obey the Arrhenius model [43, 54] given by:

$$\sigma_{dc} = \sigma_o \, Exp\,(-\frac{E_a}{K_B T}) \qquad (4)$$

where σ_o is the pre-exponential factor, E_a is the activation energy, K_B is Boltzmann constant, and T is absolute temperature. Figure 13 represent the Arrhenius plot of $\log \sigma_{dc}$ versus $1000/T$ for CPT1 composite sample. An increase in temperature caused the increase in free volume due to the segmental motion of the polymer chains, which facilitate the migration of ionic-charge carriers [36,55]. The value

of activation energy of CPT1 film is evaluated from the linear slope of the fitted Arrhenius plot and found to be equal to1.13 eV.

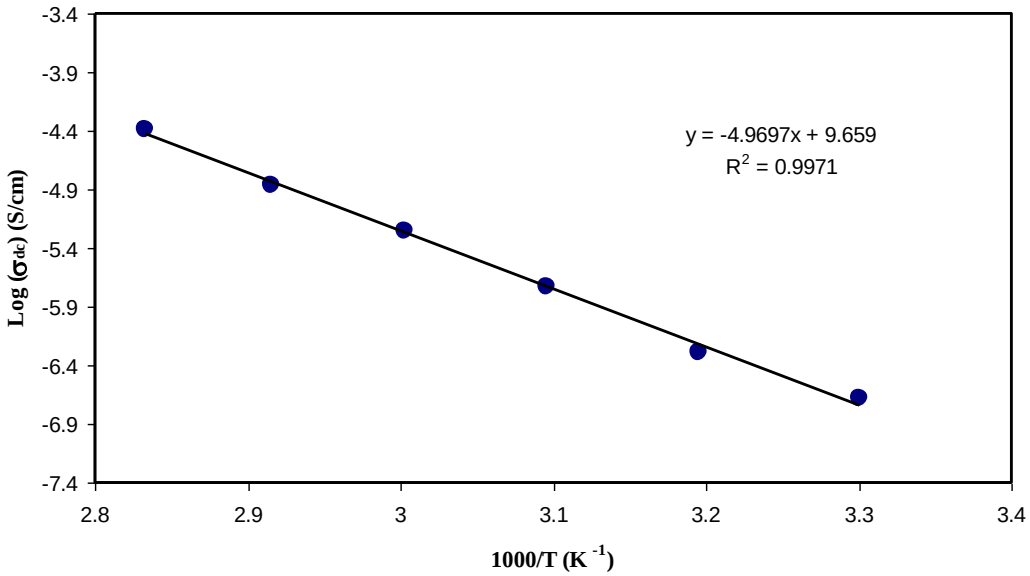

Figure 13. Arrhenius plot ($\log \sigma_{dc}$ versus $1000/T$) for CPT1 composite film.

To achieve more information about the relaxation dynamics $\tan \delta$ againsfrequeny was plotted at selected temperatures for CPT1. It can be observed from Figure 14 that $\tan \delta$ increases with frequency, passes throughout a maximum value and after that decreases. It is clear from the figure that the maximum $(\tan \delta)_{max}$ shifts to higher frequencies as the temperature increases. The moves of tanδ peaks with temperature imply that the relaxation dynamics of ions is thermally activated in the studied sample [45, 56]. In polymer electrolytes with noticeable conductivity, dielectric relaxation peaks attributable to permanent dipoles could be covered by mobile charged species contribute to DC conductivity in the material and as a result the low frequency relaxation peaks cannot be appear as observed in ε" plot [57]. The $\tan \delta$ shape of Fig. 14 can be discussed based on the Koops phenomenological model [58]. According to this model, $\tan \delta$ amplify with raise in frequency, and illustrates a maximum at exact frequencies for selected temperatures. This is related to the reality that the ohmic component of current boosts more suddenly than its capacitive component. At higher frequencies $\tan \delta$ fall with rising frequency because the ohmic component of current is basically frequency independent and the capacitive component enlarge in proportion to frequency [58, 59]. The broad shapes of the tanδ peak point out that the relaxation process is non-Debye relaxation. The raise of $\tan \delta$ intensity from 2.4 to 4.7 with temperature might be endorsed to the diminish in resistivity of composite film [60].

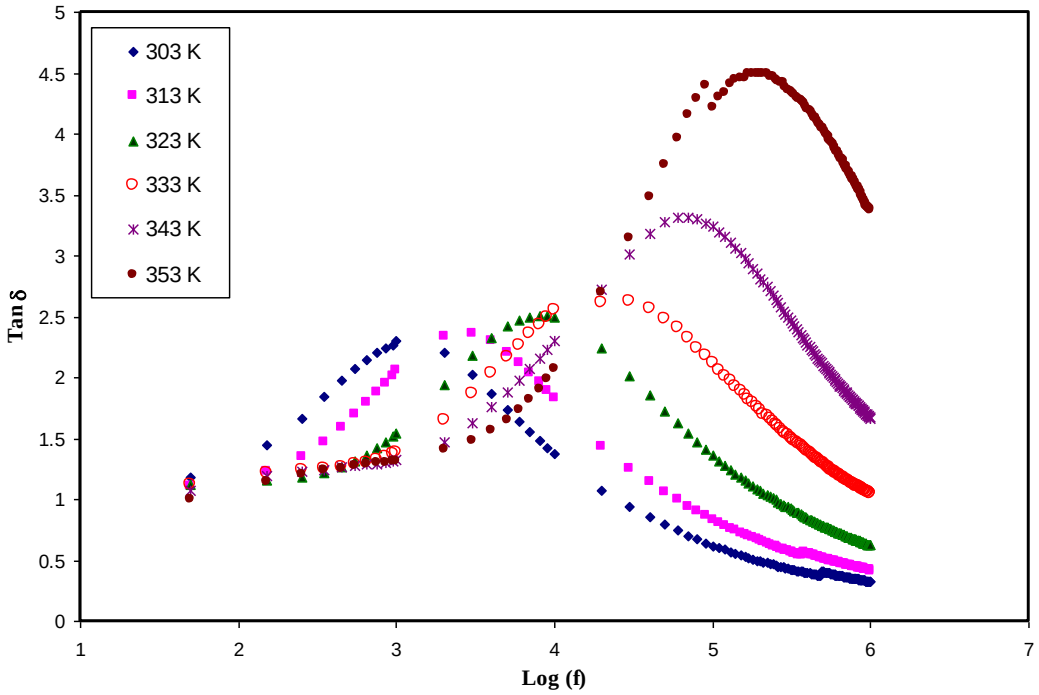

Figure 14. Frequency and temperature dependence of dielectric loss tangent (tan δ) for CPT1 composite film.

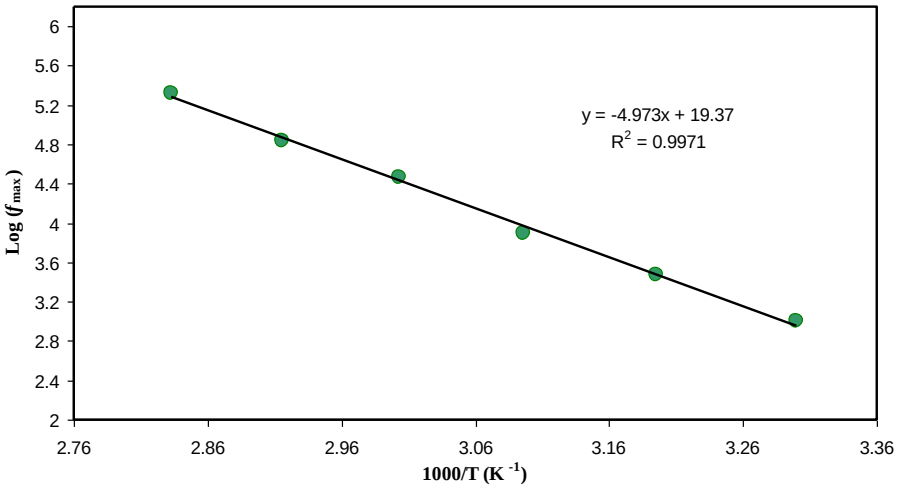

Figure 15. variation of $\log(f_{max})$ against $1000/T$ for CPT1 composite film.

The frequency associated with each peak is known as relaxation frequency and gives the most probable relaxation time for ions from the relation $2\pi f_{max} = 1/\tau$, here τ is the relaxation time and f_{max} is the frequency corresponding to $(\tan\delta)_{max}$. The reciprocal temperature variation of $\log(f_{max})$ is shown in Figure 15. The frequency-temperature relationship satisfies the Arrhenius behavior with the activation energy for relaxation equal to $E_a = 1.12\ eV$. This activation energy is close to the activation energy for conduction that obtained from plots of $\log(\sigma)$ against $1000/T(1.13\ eV)$. This is probably because the contribution to both the relaxation and conductivity attributed to the same mechanism [61]. in view of the fact that the plots of conductivity and peak frequency versus temperature follows Arrhenius, it can be realized that the behaviour of the ion transport in the composite electrolyte film

takes place through the hopping among the neighbouring vacant sites. The increase in temperature supports the segmental motions which permits the faster ionic movement or offers pathways for ions to move, hence boosts the conductivity [62, 63]. The linear character of DC conductivity with temperature means that ion transport occurs through the thermally activated processes [64].

4. CONCLUSIONS

In the current work the role of titanium dioxide (TiO_2) filler on dielectric and conductivity properties of chitosan (CS) based solid polymer electrolytes (SPEs) were investigated at various temperatures. To prepare CS based SPEs fixed amount of ammonium triflate ($NH_4CF_3SO_3$) was dissolved in CS solution and then various amount of TiO_2 was added to CS: $NH_4CF_3SO_3$ solution. The films of composite electrolytes were obtained by solution cast technique. The results showed that dielectric properties of composite electrolytes have been improved up to 1 wt.% of TiO_2 and their values are found to be temperature dependent. The composite film incorporated with 1 wt.% of TiO_2 exhibits a smallest bulk resistance. The *M''* parameter against frequency shows asymmetric single relaxation peak which reveal the non-Debye relaxation type. The ac conductivity spectra were used to obtain the DC conductivity values at ambient temperature. The temperature dependent DC conductivity was found to follow Arrhenius behaviour. The obtained value of activation energies from DC conductivity is found to be comparable to that calculated from relaxation time. The single value of activation energy obtained from the Arrhenius plot indicates one conduction mechanism involved in the present system.

ACKNOWLEDGMENTS
S.B. Aziz and O.G. Abdullah thanks the University of Sulaimani, and the Komar University of Science and Technology for providing the facility and financial support to carry out this work. The authors appreciatively acknowledge the financial support from the Kurdistan National Research Council (KNRC)- Ministry of Higher Education and Scientific Research-KRG for this research project.

References

1. T.H. Le, Y. Kim, and H. Yoon, *Polymers* 9 (2017) 150.
2. M.H. Suhail, A.A. Ramadan, S.B. Aziz, and O.G. Abdullah, *J. Sci. Adv. Mater. Devices*, 2 (2017) 301.
3. T.Y. Kim, S. Lee, D.Jeong, T.K. Lee, B.S. Kim, S.Chae, and Y.S. Kang, *ACS Appl. Energy Mater.*1 (2018) 290.
4. S.B. Aziz, O.G. Abdullah, M.A. Rasheed, and H.M. Ahmed, *Polymers*, 9 (2017) 187.
5. Y.A.K. Salman, O.G. Abdullah, R.R. Hanna, and S.B. Aziz, *Int. J. Electrochem. Sci.*, 13 (2018) 3185.
6. O.G. Abdullah, R.R. Hanna, Y.A.K. Salman, and S.B. Aziz, *J. Inorg. Organomet. Polym. Mater.*28 (2018) 1432.
7. S.B. Aziz, O.G. Abdullah, S.A. Hussein, and H.M. Ahmed, *Polymers*, 9 (2017) 622.
8. M. Hdidar, S. Chouikhi, A. Fattoum, M. Arous, A. Kallel, *J. Alloy. Compd.* 750 (2018) 375.
9. K. S. Hemalatha, K.Rukmani, N.Suriyamurthy, and B.M.Nagabhushana, *Mater. Res. Bull.*, 51 (2014) 438.

10. S. B. Aziz, H. M. Ahmed, A. M. Hussein, A. B. Fathulla, R. M. Wsw, R. T. Hussein, *J. Mater. Sci: Mater. Electron.,* 26 (2015) 8022
11. S.B. Aziz, M. A. Rasheed, A. M. Hussein, H. M. Ahmed, *Mater. Sci. Semicond. Process.,* 71 (2017) 197
12. S.B. Aziz, *Nanomaterials,* 7 (2017) 444
13. S.B. Aziz, Omed Gh Abdullah, Mariwan A Rasheed, *J. Appl. Polym. Sci.,* 134 (2017) 44847
14. S. B. Aziz, Z. H. Z Abidin, M.F.Z. Kadir, *Phys. Scr.,* 90 (2015) 035808 (9pp)
15. S.P. Mondal, H. Mullick, T. Lavanya, A. Dhar, S.K. Ray, and S.K. Lahiri, *J. Appl. Phys.,* 102 (2007) 064305.
16. J. Lee, D. Bhattacharyya, A. J. Easteal, and J. B. Metson, *Curr. Appl. Phys*., 8 (2008) 42.
17. G. Pathak, S. Pandey, R. Katiyar, A. Srivastava, R. Dabrowski, K. Garbat, and R. Manohar, *J. Lumin.*, 192 (2017) 33.
18. Y. Bai, I.M. Sero, F.D. Angelis,J. Bisquert, and P. Wang, *Chem. Rev.*, 114 (2014) 10095.
19. T. Hitosugi, N. Yamada, S. Nakao, Y. Hirose,and T. Hasegawa, *Phys. Status Solidi A*, 207 (2010) 1529.
20. X. Wang, and Z.M. Wang, High-efficiency solar cell, International Publishing Switzerland (2014).
21. A.S.A. Khiar, R. Puteh, and A.K. Arof, *phys. stat. sol.,* 203(2006) 534.
22. S. B. Aziz, W. O. Karim, K. W. Qadir, Q. Zafar, *Int. J. Electrochem. Sci.,*13 (2018) 6112.
23. S. B. Aziz, *Bull. Mater. Sci*., 38 (2015) 1597.
24. S. B. Aziz, *Appl. Phys. A, 122* (2016) 706.
25. S. B. Aziz, *Iran. Polym. J*., 22 (2013) 877.
26. S. B. Aziz, *J. Inorg. Organomet. Polym Mater.*, 28 (2018) 1942.
27. S. B. Aziz, R. M. Abdullah, *Electrochim. Acta,* 285 (2018) 30.
28. S. B. Aziz and Z.H.Z. Abidin, *J. Appl. Polym. Sci.*,132 (2015) 41774.
29. S. B. Aziz and Z.H.Z. Abidin, *Mater. Chem. Phys.*, 144 (2014) 280.
30. S. Ibrahim, S. M. M. Yasin, N. M. Nee, R. Ahmad, and M.R. Johan, *Solid State Commun.,* 152 (2012) 426.
31. D. Koch, and S. Manzhos, *J. Phys. Chem. Lett.,* 8 (2017) 1593.
32. S. B. Aziz, *Adv. Mater. Sci. Eng.*, 2016 (2016), Article ID 2527013, 11 pages, http://dx.doi.org/10.1155/2016/2527013
33. S. B. Aziz, O. G. Abdullah, S. R. Saeed, and H.M. Ahmed, *Int. J. Electrochem. Sci.* 13 (2018) 3812.
34. D. K. Pradhan, R.N.P. Choudhary, and B.K. Samantaray, *Int. J. Electrochem. Sci.* 3, 597 (2008).
35. O. G. Abdullah, R.R. Hanna, and Y.A.K. Salman, *J. Mater. Sci. Mater. Electron.* 28 (2017) 10283.
36. S. Ramesh, and O.P. Ling, *Polym. Chem.* 1 (2010) 702.
37. S. B. Aziz, O.G. Abdullah, and M.A. Rasheed, *J. Mater. Sci. Mater. Electron.* 28 (2017) 12873.
38. K.S. Hemalatha, G. Sriprakash, M.V.N.A. Prasad, R. Damle, and K. Rukmani, *J. Appl. Phys.* 118 (2015) 154103.
39. B. Behera, P. Nayak, and R.N.P. Choudhary, *J. Alloy. Compd.* 436 (2007) 226.
40. S. Sen, R.N.P. Choudhary, and P. Pramanik, *Physica B*, 387 (2007) 56.
41. A. K. Jonscher, *Nature,* 267 (1977) 673.
42. S. B. Aziz, O.G. Abdullah, and S.A. Hussein, *J. Electron. Mater.*, 47 (2018) 3800.
43. O. G. Abdullah, S.B. Aziz, and M.A. Rasheed, *Ionics*, 24 (2018) 777.
44. T. T. N. Vu, G. Teyssedre, S.L. Roy, and C. Laurent, *Technologies*, 5 (2017) 27.
45. V. M. Mohan, W. Qiu, J. Shen, and W. Chen, *J. Polym. Res.*, 17 (2010) 143.
46. O. G. Abdullah, Y.A.K. Salman, and S.A. Saleem, *J. Mater. Sci. Mater. Electron.*, 27 (2016) 3591.
47. V. Senthil, T. Badapanda, S.N. Kumar, P. Kumar, and S. Panigrahi, *J. Polym. Res.* 19 (2012) 9838.
48. O. G. Abdullah, and S.A. Saleem, *J. Electron. Mater.*, 45 (2016) 5910.
49. S. B. Aziz and Z. H. Z. Abidin, *J. Soft Matter*, 2013 (2013), Article ID 323868, 8 pages, http://dx.doi.org/10.1155/2013/323868

50. M. Samet, V. Levchenko, G. Boiteux, G. Seytre, A. Kallel, and A. Serghei, *J. Chem. Phys.*, 142 (2015) 194703.
51. S. B. Aziz, R. M. Abdullah, M. A. Rasheed, and H. M. Ahmed, *Polymers*, 9 (2017) 338
52. S. B. Aziz, Z. H. Z. Abidin, A. K. Arof, *eXPRESS Polym. Lett.*, 4 (2010) 300.
53. A. Arya, M. Sadiq, and A. L. Sharma, *Ionics*, 24 (2018) 2295.
54. S. B. Aziz, M. F. Z. Kadir, and Z. H. Z. Abidin, *Int. J. Electrochem. Sci.*, 11 (2016) 9228.
55. S. B. Aziz, Z. H. Z. Abidin, A. K. Arof, *Physica B* 405(2010) 4429.
56. L. Fan, Z. Dang, G. Wei, C.W. Nan, and M. Li, *Mater. Sci. Eng. B,* 99 (2003) 340.
57. P. A. R. D. Jayathilaka, M. A. K. L. Dissanayake, I. Albinsson, and B.E. Mellander, *Solid State Ionics,* 156 (2003) 179.
58. P. Khatri, B. Behera, V. Srinivas, and R.N.P. Choudhary, *Curr. Appl. Phys.*, 9 (2009) 515.
59. B. Louati, F. Hlel, K. Guidara, *J. Alloy. Compd.*, 486 (2009) 299.
60. N.H. Idris, H.B. Senin, and A.K. Arof, *Ionics*, 13 (2007) 213.
61. T.M.W.J. Bandara, B.E. Mellander, I. Albinsson, and M.A.K.L. Dissanayake, *Solid State Ionics,* 180 (2009) 362.
62. N. S. Salleh, S. B. Aziz, Z. Aspanut, M. F. Z. Kadir, Ionics, 22 (2016) 2157.
63. S. B. Aziz, T. J. Woo, M. F. Z. Kadir, H. M. Ahmed, *J. Sci.: Adv. Mater. Devices*, 3 (2018) 1-17.
64. S. B. Aziz, M.G. Faraj, O. Gh. Abdullah, *Scientific Reports* 8 (2018) 14308. DOI:10.1038/s41598-018-32662-1